Proceedings of the
2007 IEEE Intelligent Vehicles Symposium
Istanbul, Turkey, June 13-15, 2007

Coordination of Vehicle Motion and Energy Management Control Systems for Wheel Motor Driven Vehicles

Leo Laine and Jonas Fredriksson

Abstract— **This paper shows how smooth coordination of vehicle motion controller and energy management can be achieved when control allocation is used for over-actuated ground vehicles. The ground vehicle studied here is equipped with four electric wheel motors, four disc brakes, and front and rear steering. This gives a total of ten input signals to control the desired vehicle motion in longitudinal-, lateral-, and yaw-direction. Simulations show that the desired input signals from energy management and steering can be fulfilled, but when needed the actual input signals for the motion actuators are smoothly diverted from the desired input signals due to vehicle stability reasons and/or saturation of the actuators.**

I. INTRODUCTION

If or when the era of the combustion engine within automotive applications ends or becomes less dominating, the propulsion system of the vehicles will most likely be electrified. The first transition away from the combustion engine dependence has already started, with the launch of the Toyota Prius in 1997. The car is equipped with the Toyota Hybrid System (THS) [1] which combines the combustion engine with electric motors. This allows the combustion engine to be downsized. The Prius has been followed by several other commercially available hybrid electric vehicles. The final transition will come when the prices for oil will become too high or when environmental legislations demands for alternative fuels. One possible option to meet the new demands is the fuel cell (fc) which converts hydrogen and oxygen into electricity and water.

When automotive vehicles become more electrified many hydraulical and mechanical functions can be replaced by electrical ones [2]. In this paper a future vehicle configuration is studied which has replaced the combustion engine with four electric motors mounted on each wheel. The motors are propelled by a fuel cell in combination with a battery. The mechanical braking is assumed to be independently controlled, and the steering is assumed to be by-wire, with independent front and rear steering. Clearly, by introducing so many motion actuators the desired global longitudinal-, lateral-, and yaw- motion of the vehicle can be realized in many different ways by using the available motion actuators. This type of systems are called over-actuated systems.

This work is supported by the Swedish national research programme Gröna Bilen/FCHEV. Gröna Bilen is financed by Swedish automotive industry and the Swedish research foundation Vinnova.

L. Laine is with the Department of Applied Mechanics, Div. of Vehicle Safety and Vehicle Dynamics, SAFER, Chalmers University of Technology, SE-417 56 Göteborg, Sweden, leo.laine@chalmers.se

J. Fredriksson is with the Department of Signals and Systems, Div. of Automatic Control, Automation and Mechatronics, Chalmers University of Technology, jonas.fredriksson@chalmers.se

In this paper it is shown how control allocation [3] can be a viable option to ease the control design of over-actuated ground vehicle systems when both the vehicle motion and energy management are considered. The outline of the paper is as follows: Section I-A gives a background of using control allocation within the control system. Section II explains how the ground vehicle is modelled. Section III describes the control design. Section IV and V explains the simulated cases and the results. Finally in Section VI concluding remarks are made.

A. Background

One promising way to manage the coordination of over-actuated systems is to use control allocation. Control allocation deals with the problem of distributing the control demand within an available set of actuators. The control demand $v \in R^k$ is mapped onto the true control input of the actuators $v \mapsto u$, where $u \in R^m$ and $k < m$. The allocation problem lies in that there are several input sets of u that can give the control demand v. The control allocation problem is posed as a constrained optimization problem which provides automatic redistribution of the control effort when one actuator saturates in position or in rate. Control allocation has been used successfully in flight applications [3], marine vessels [4], [5], and for ground vehicles [6], [7], [8]. In [6]-[8] the mechanical brakes and steering were in focus without direct considerations to the actuator limits.

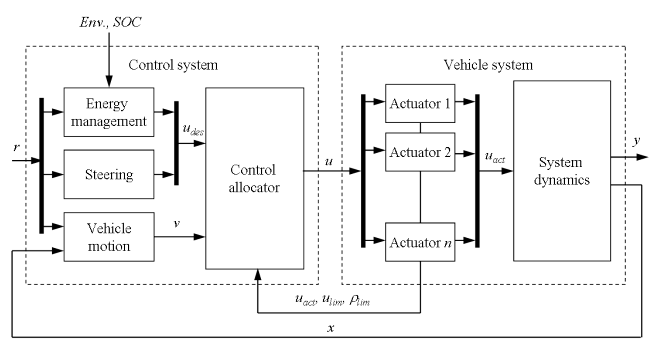

Fig. 1. Suggested control system architecture when control allocation is used for Hybrid Electric Vehicle systems.

In earlier work by the authors, [9] and [10], it was shown how the control system can be made reusable for different vehicle configurations when one separates the control law from the control allocation for achieving the vehicle motion. Wheel force limits in combination with constraints due to vehicle configuration allowed a reusable structure. Here, in

1-4244-1068-1/07/$25.00 ©2007 IEEE.

this paper the limits are taken one step further, actuator position and rate of change limits in combination with tyre force limits are considered as constraints for the control allocator. Additionally, it is here shown that the proposed control system also allows separate control laws for energy management and steering in addition to vehicle motion as shown in Fig. 1. The authors have not found any work showing how one smoothly combines energy management and vehicle motion control for a HEV by using constrained control allocation with optimization formulation.

II. SYSTEM MODELLING

The system modelling is separated into three parts:

A. Chassis including tyre dynamics

The chassis model is a so-called two track model and has five degree of freedom: longitudinal-, lateral-, yaw-, roll-, and pitch motion. The model aims at being good enough in representing the chassis dynamics on a flat surface. The SAE standard [11] has provided the main guidance for defining the axis orientations. A brush tyre model [12] is used together with dynamic relaxation to describe the tyre dynamics. The used chassis parameters are comparable to a commercial medium sized sedan car.

B. Power Supply including energy buffer

Here one type of Power Supply system is studied, a series vehicle configuration with a fuel cell and a buffer. The fuel cell can deliver a continuous output power of 30 kW, the power is sufficient to overcome the resistance forces at a constant speed of 130 km/h for a medium sized sedan car. Fig. 2 shows the efficiency curve as a function of output power for the fuel cell model, which also includes parasitic losses. One can see that output power lower than 10 kW yields bad efficiency and should be avoided. Good efficiency is found between 10 and 40 kW. The optimal output power from the fuel cell is about 20 to 30 kW.

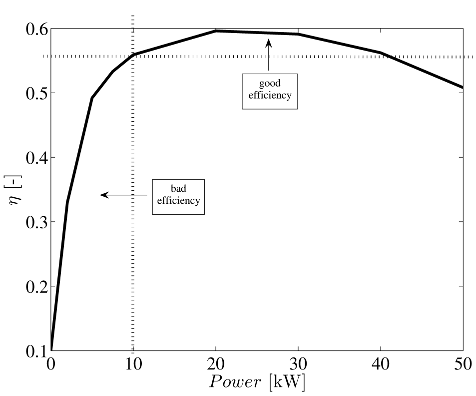

Fig. 2. Efficiency as a function of output power for simulated fuel cell.

A fuel cell stack such as Proton Exchange Membrane (PEM) can deliver short pulses of output power before the compressor reaches desired speed. This can be seen as there are two time constants one 'instantaneous' and one 'steady state' [13]. The experimental results in [13] showed that the instantaneous time constant was in the order of 11 μs and the steady state about 400 ms to reach 63 percent of its final value. However, the time constants will get shorter if the fuel cell is already operating with high output power as a initial condition. Here only a simplified first order model is used for the fuel cell output power with a time constant of 400 ms which then neglects the instantaneous time constant.

An energy buffer is needed to be able to handle peak accelerations and store regenerated brake energy. According to [14] the most efficient buffer is a battery when performance, such as peak acceleration, towing, and price are compared for battery, ultracapacitors, and a combination of battery and ultracapacitors. A battery with a high energy density allows the fuel cell to work at efficient operating points or even to be shut down when low output power is needed.

The peak output power is 175 kW of which 40 kW is from fuel cell and 135 kW is from buffer. The buffer power is achieved by selecting a battery mass of 90 kg with 1500 W/kg charge and discharge power density. The selected power density is based upon that Ni/MH batteries have about 1200 W/kg and Li-ion about 2000 W/kg [15]. However the Li-ion have still not had a break through in automotive applications due to problems in cost, life, abuse tolerance, and low temperature performance [15]. The operating State of Charge (SOC) window was set to $SOC_{min} = 40$ % and $SOC_{max} = 90$ %.

C. Motion actuator dynamics

The series HEV has wheel motors mounted on each wheel with maximum output power of 40 kW, which gives four control inputs. Additionally, each wheel has individually controlled disc brakes, which give additional four control inputs. The actual torque limits delivered for the actuators are modelled by thermal lumped mass models for both electric motors and mechanical brakes. The temperature model tightens the actual limits due to overheating of the electric motor windings and the permanent magnets. For the mechanical brakes the friction is temperature dependent. Additionally the rotational speed is constraining the electric motor. The actuator limits from electric motors $\overline{u}_{\mathrm{el},i}$ and mechanical brakes $\overline{u}_{\mathrm{mech},i}$ can be expressed as

$$\begin{aligned} \underline{u}_{\mathrm{el},i}(\omega_i, T_i) \leq u_{\mathrm{el},i} \leq \overline{u}_{\mathrm{el},i}(\omega_i, T_i) \\ \underline{u}_{\mathrm{mech},i}(T_i) \leq u_{\mathrm{mech},i} \leq \overline{u}_{\mathrm{mech},i}(T_i) \end{aligned} \tag{1}$$

where ω_i and T_i are the angular velocity and temperature of the actuator. The actuator models give also information of the rate of change limits. Finally, steering is seen as steer by wire by front and rear rack steer which gives two additional control inputs, i.e. the configuration has a total of 10 control inputs.

III. CONTROL DESIGN

Independently of the specific applications studied, a class of nonlinear systems can be described in the affine form

$$\dot{x} = f(x) + g(x)u \tag{2}$$

$$y = h(x) \tag{3}$$

Control allocation can be applied if the control input can be perturbed without affecting the system dynamics. The system can therefore rewritten as

$$\dot{x} = f(x) + v \tag{4}$$

$$y = h(x) \tag{5}$$

where $v = g(x)u$, v is also called the virtual control input.

The control design can be divided into two steps. The first step is to design a control law that controls the net effort v. The second step is to design a control allocator that maps the net effort of virtual control input to true control input, $v(t) \mapsto u(t)$. Unfortunately, the mapping of the net effort to the true control signal is complicated since the $g(x)$-matrix is not invertible. Using a pseudo-inverse to find a solution could be one way of solving this. However, this could lead to an unrealistic solutions since the true control signals are limited by several different constraints, see Eq. 1. Instead a constrained optimization problem is proposed and solved.

The chassis system can be written as

$$M\dot{x} = f(x) + g(x)u \tag{6}$$

$$y = h(x) \tag{7}$$

where M is the mass matrix

$$M = \begin{bmatrix} m & 0 & 0 \\ 0 & m & 0 \\ 0 & 0 & I_z \end{bmatrix}$$

and

$$f(x) = \begin{bmatrix} m x_2 x_3 - D_1 x_1 - D_2 m \operatorname{sgn}(x_1) x_1^2 \\ -m x_1 x_3 - C_\alpha \frac{8x_1(2x_2 + (L_f - L_r)x_3)}{4x_1^2 - b_t^2 x_3^2} \\ -L_f C_\alpha \frac{8x_1(2x_2 + L_f x_3)}{4x_1^2 - b_t x_3^2} + L_r C_\alpha \frac{8x_1(2x_2 - L_r x_3)}{4x_1^2 - b_t x_3^2} \end{bmatrix} \tag{8}$$

$$g(x)u = \begin{bmatrix} \sum_{i=1}^{4} F_{x,i} \\ C_\alpha \sum_{i=1}^{4} \delta_i \\ L_f C_\alpha \sum_{i=1}^{2} \delta_i - L_r C_\alpha \sum_{i=3}^{4} \delta_i + \frac{B_t}{2} \sum_{i=3}^{4} (-1)^{1+i} F_{x,i} \end{bmatrix} \tag{9}$$

$$h(x) = \begin{bmatrix} x_1 & x_2 & x_3 \end{bmatrix}^T \tag{10}$$

where x_1, x_2, and x_3 correspond to longitudinal-, lateral- and yaw- velocity of the vehicle. Here, a linear tyre force model of type $F_{y,i} = C_\alpha \alpha_i$ is assumed and that one can split the lateral tyre forces into steer angle and vehicle state dependence, $F_{y,i} = F_{y,i}(\delta_i) + F_{y,i}(x)$. The lateral tyre forces depending on vehicle states $F_{y,i}(x)$ and depending on steering angles $F_{y,i}(\delta_i)$ can therefore be separated into $f(x)$ and $g(x)u$, respectively. D_1 and D_2 are constants related to aerodynamical and rolling resistance. Since the mass matrix is invertible, the system can be written in affine form. Looking at $g(x)u$ in Eq. 9 it corresponds to longitudinal and lateral global forces and yaw moment of the vehicle and can therefore be considered as the virtual control input v.

A. Control Law for Vehicle Motion

The purpose of the vehicle motion controller is to follow a desired trajectory interpreted from the driver's steering actions. The controller is based on feedback linearization, see e.g. [16]. The idea with feedback linearization is to transform the nonlinear system into a linear one, so that linear techniques can be used. In its simplest form it can be seen as a way to cancel the nonlinearities by a nonlinear state feedback. Looking at the system, it can be noticed that the first term on the right hand side of (6) is the only one including the nonlinearities of the system. If the non-linear term, $f(x)$, is cancelled, the multi-input, multi-output (MIMO)-system becomes linear. Furthermore, by cancelling $f(x)$ the MIMO-system becomes decoupled. Then, using a PI-controller, the control law becomes:

$$v = -f(x) + K_p e + K_i \int_0^t e \, d\tau \tag{11}$$

where e is the error between the desired vehicle motion and the vehicle's actual motion. The design parameters for the PI-controllers, K_p and K_i, are chosen as

$$K_i = 20 \begin{bmatrix} 0.2m & 0 & 0 \\ 0 & 0.7m & 0 \\ 0 & 0 & 1.5I_z \end{bmatrix} \tag{12}$$

$$K_p = \frac{2}{3} m \sqrt{K_i \begin{bmatrix} \frac{16}{m} & 0 & 0 \\ 0 & \frac{1}{m} & 0 \\ 0 & 0 & \frac{1}{I_z} \end{bmatrix}} \tag{13}$$

To handle saturation of actuators the PI-controllers are extended with anti-windup based on back calculation [17].

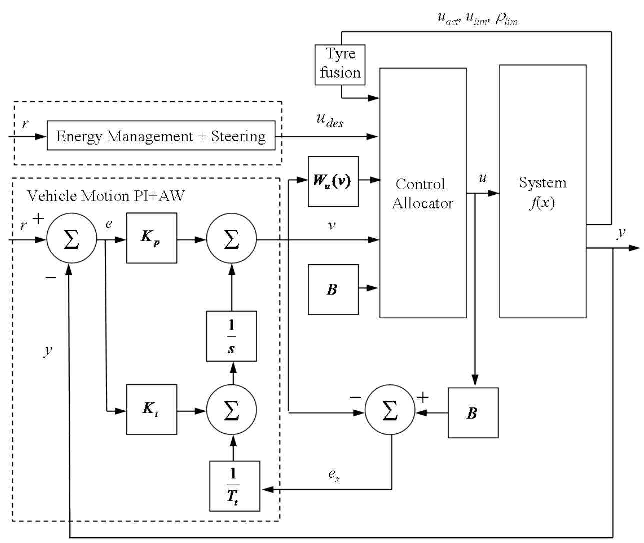

Fig. 3. Control Design illustration with focus on control law for vehicle motion, a PI controller with Anti-Windup strategy that decides the virtual control input $v(t)$ which is then mapped onto the true control input $u(t)$ by the control allocator, where $g(x)u \approx Bu$. The control allocator uses a weight scheduled weighting matrix $W_u(v_1)$.

B. Control Law for Energy Management

The objective of the energy management algorithm is to minimize fuel consumption and assure optimal power availability at any time. The used and implemented energy management strategy is inspired by [18]. It uses a finite state machine which distinguishes between four driving modes:

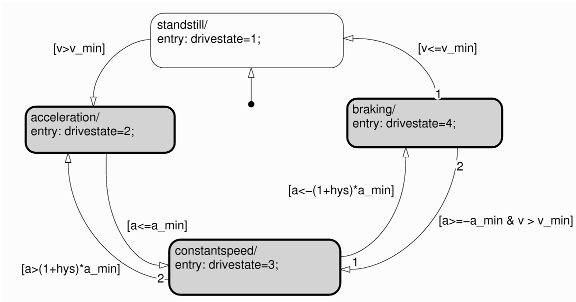

Fig. 4. Driving modes used for Energy Management, inspired by [18].

standstill, acceleration, constant speed, and braking, which are based upon speed and acceleration as illustrated in Fig. 4.

During the four modes different strategies are applied for how the total power demand is divided between the fuel cell and the battery. As shown in Fig. 2 it is important to avoid bad efficiency of the fuel cell as much as possible which is found during low output power less than 10 kW and at maximum output power above 40 kW. Secondly the steady state rise time of output power for a fuel cell is about 400 ms which leads to that highly transient power demands should be delivered by the battery. These two design criteria are considered for the control laws used within the four modes:

1) Standstill:

$$P_{fc} = \begin{cases} P_{fc,opt}, \text{ if } SOC \leq SOC_{min} \\ 0, \text{ else} \end{cases} \tag{14}$$

$$P_{bf} = \begin{cases} -P_{fc}, \text{ if } SOC \leq SOC_{min} \\ 0, \text{ else} \end{cases} \tag{15}$$

2) Acceleration:

$$P_{fc} = \begin{cases} \min\left(\hat{P}_{dem}, 40\right), \text{ if } 10 \text{ kW} \leq P_{dem} \\ 0, \text{ else} \end{cases} \tag{16}$$

$$P_{bf} = \begin{cases} P_{dem} - P_{fc}, \text{ if } 10 \text{ kW} \leq P_{dem} \\ P_{dem}, \text{ else} \end{cases} \tag{17}$$

3) Constant speed:

$$P_{fc} = \begin{cases} P_{fc,opt}, \text{ if } SOC \leq SOC_{min} \ \& \ 10 \text{ kW} \geq P_{dem} \\ \min\left(\hat{P}_{dem}, 40\right), \text{ if } 10 \text{ kW} \leq P_{dem} \\ 0, \text{ else} \end{cases} \tag{18}$$

$$P_{bf} = \begin{cases} P_{dem} - P_{fc}, \text{ if } 10 \text{ kW} \leq P_{dem} \\ P_{dem} - P_{fc}, \text{ if } SOC \leq SOC_{min} \ \& \ 10 \text{ kW} \leq P_{dem} \\ P_{dem}, \text{ else} \end{cases} \tag{19}$$

4) Braking:

$$P_{bf} = \begin{cases} P_{dem}, \text{ if } |P_{dem}| \leq 134 \text{ kW} \ \& \ SOC \leq SOC_{max} \\ P_{bf,max}, \text{ if } |P_{dem}| \geq 134 \text{ kW} \ \& \ SOC \leq SOC_{max} \\ 0, \text{ else} \end{cases} \tag{20}$$

$$P_{mb} = \begin{cases} P_{dem} - P_{bf,max}, \text{ if } |P_{dem}| \geq 134 \text{ kW} \ \& \ SOC \leq SOC_{max} \\ P_{dem}, \text{ if } SOC \geq SOC_{max} \\ 0, \text{ else.} \end{cases} \tag{21}$$

where P_{fc}, P_{bf}, and P_{mb} are fuel cell, buffer, and mechanical brake output power. $P_{fc,opt} = 20$ kW is the optimal output power of fc, see also Fig. 2. P_{dem} is the power demand. $\hat{P}_{dem}$ is the low pass filtered power demand with cutoff frequency of 2 rad/s. The low pass filtering is used for achieving an output within range of the slow response of the fuel cell. The power demand of the vehicle is calculated with the following expression

$$P_{dem} = P_{acc} + P_{loss} + P_{aux}. \tag{22}$$

Where $P_{acc} = mav$ is the acceleration power needed. $P_{loss} = D_1 v + D_2 v^2$ is the rolling and air resistance, and P_{aux} is the auxiliary power needed for other electric loads such as air conditioner, here assumed to be a constant of 0.5 kW.

The desired torque on the specific electrical and mechanical actuators are assumed to be evenly distributed

$$\tau_{wm_i} = \frac{\left(P_{fc} + P_{bf}\right) R_w}{4 v_x r_{fg}} \tag{23}$$

$$\tau_{mb_i} = \frac{P_{mb} R_w}{4 v_x} \tag{24}$$

where i is the wheel number, R_w is the wheel radius, and r_{fg} is the final gear of the electric wheel motor. For low vehicle velocities $v_x < 0.1$ m/s the desired torques are set equal to zero and solely solved by the vehicle motion control law and the control allocator. These desired torques will give the first eight positions of the vector

$$u_{des} = \begin{bmatrix} \tau_{wm_1} & \tau_{wm_2} & \tau_{wm_3} & \tau_{wm_4} & \tau_{mb_1} & \tau_{mb_2} & \tau_{mb_3} & \tau_{mb_4} & \delta_f & \delta_r \end{bmatrix}^T, \tag{25}$$

see also Fig. 3.

C. Control Law for Steering

The reference model within the driver interpreter of the vehicle is assumed to deliver the desired reference signal $r = \begin{bmatrix} v_x & v_y & \omega_z \end{bmatrix}$, vehicle's longitudinal-, lateral-, and yaw-velocity, to the steering function, see also Fig. 1. Here the inverse dynamics of a linear bicycle model is used to derive the desired front and rear steering angle inputs δ_f and δ_r. The linear bicycle model assumes: v_x to be constant, steering angles to be small, and a linear tyre force model $F_y = C_\alpha \alpha$. The model can be then expressed as

$$\dot{x}_{steer} = A x_{steer} + B u_{steer} \tag{26}$$

$$A = -\begin{bmatrix} \frac{C_{\alpha_f} + C_{\alpha_r}}{m v_x} & v_x + \frac{L_f C_{\alpha_f} - L_r C_{\alpha_r}}{m v_x} \\ \frac{L_f C_{\alpha_f} - L_r C_{\alpha_r}}{I_z v_x} & \frac{L_f^2 C_{\alpha_f} + L_r^2 C_{\alpha_r}}{I_z v_x} \end{bmatrix} \tag{27}$$

$$B = \begin{bmatrix} \frac{C_{\alpha_f}}{m} & \frac{C_{\alpha_r}}{m} \\ \frac{L_f C_{\alpha_f}}{I_z} & -\frac{L_r C_{\alpha_r}}{I_z} \end{bmatrix} \tag{28}$$

where $x_{steer} = \begin{bmatrix} v_y & \omega_z \end{bmatrix}$ and $u_{steer} = \begin{bmatrix} \delta_f & \delta_r \end{bmatrix}$. By assuming that the desired accelerations $\hat{\dot{x}}_{steer}$ can be estimated by time discrete differentiation of the reference signal $\hat{\dot{r}} = \frac{r(k+1) - r(k)}{t(k+1) - t(k)}$, the needed input can be solved by

$$u_{steer} = B^{-1}\left(\hat{\dot{x}}_{steer} - A x_{steer}\right) \tag{29}$$

where B^{-1} exists because B has full rank. For low longitudinal velocities v_x the A matrix becomes singular, however for low velocities the steering is more a geometrical problem such as $\delta_f = L_f/R$ and $\delta_r = -L_r/R$, where R is the turning radius. Eq. 29 gives the last two positions of the vector u_{des}, Eq. 25, see also Fig. 3.

D. Control Allocation

The second step in the control design is to create the control allocator. The key issue is how to select the control input set u from all possible combinations. Here, a constrained control allocation with mixed optimization is used to map the virtual control input $v(t)$ onto true control input $u(t)$. The virtual control input is the global longitudinal and lateral forces and the yaw moment of the vehicle $v(t) = \begin{bmatrix} F_x & F_y & M_z \end{bmatrix}^T$, which is controlled by the control law for vehicle motion, see Section III-A. Looking at the model (Eqs. 8-7) the true control signals are the longitudinal wheel forces $F_{x,i}$ and the wheel steering angles δ_i. The wheel forces are controlled by the electric motors via the driveline and the mechanical brakes. Thus the true control input is selected as $u(t) = \begin{bmatrix} \tau_{wm_1} & \tau_{wm_2} & \tau_{wm_3} & \tau_{wm_4} & \tau_{mb_1} & \tau_{mb_2} & \tau_{mb_3} & \tau_{mb_4} & \delta_f & \delta_r \end{bmatrix}^T$, where τ_i is the torque from the traction and braking actuators. i is the wheel number starting at front left, front right, rear left, and rear right. $\delta_f = \delta_1 = \delta_2$ and $\delta_r = \delta_3 = \delta_4$ are the front and rear rack steering angle were the Ackermann angle is neglected. The mapping is realised by using a control effectiveness matrix $B \in R^{k \times m}$ which describes how each actuator can contribute to the global forces and moment by $v(t) \approx Bu(t)$. According to [3] the optimal control input u can be seen as two-step optimization problem, sequential least squares (sls),

$$u = \arg \underbrace{\min}_{u \in \Omega} \| W_u (u - u_{des}) \|_p \tag{30}$$

$$\Omega = \arg \underbrace{\min}_{\underline{u} \leq u \leq \overline{u}} \| W_v (Bu - v) \|_p \tag{31}$$

where W_u and W_v are weighting matrices and u_{des} is the desired control input. The two step optimization problem is well suited for FCVs and HEVs. Eq. 31 constrains the possible set $u \in \Omega$ to only be u's that will be in nullspace of $N(Bu - v)$ or minimize the error of the desired forces, $Bu - v$, needed for fulfilling the desired motion of the vehicle. This can be seen as the vehicle motion controller. Eq. 30 minimizes the error of desired control input, $u_{des} - u$. The desired control input, u_{des}, coming from the energy management controller and the control law for steering, specifies how the electric motor(s) and the mechanical brakes should be used when optimizing onboard energy and desired vehicle steering. This can be seen as a smooth arbitration between energy management and vehicle motion control. Figure 1 shows how energy management is included in the control allocator and Fig. 3 shows how the control allocator fits in the control system in more detail. Numerically Eqs. 30- 31 can also be solved in one step, using weighted least squares (wls),

$$u = \arg \underbrace{\min}_{\underline{u} \leq u \leq \overline{u}} \| W_u (u - u_{des}) \|_p + \gamma \| W_v (Bu - v) \|_p . \tag{32}$$

where $p = 2$. Setting the weighting parameter γ to a high value gives priority to minimize the error in motion $Bu - v$.

1) Actuator limits: The control allocator receives the limits from the motion related actuators, $[\underline{u}(t), \overline{u}(t)]$ and their limits in rate of change $[\underline{\rho}, \overline{\rho}]$. This specific way of designing the control system allows the control law to be independent of the available actuators, i.e. reusable for different hardware configurations, and also allows the control allocator to handle both limits and even actuator failure. The rate limits can be rewritten as position constraints using an approximation of the time derivative. The position constraints can now be written as

$$\overline{u}(t) = \min \left(\overline{u}(t), u(t - t_T) + t_T \overline{\rho} \right) \tag{33}$$

$$\underline{u}(t) = \max \left(\underline{u}(t), u(t - t_T) + t_T \underline{\rho} \right) \tag{34}$$

where t_T is the sampling time of the control allocator.

In a ground vehicle the limits of the control input must also consider the force limits of each wheel. The longitudinal force limit $F_{x,lim,i}$ is a function of the normal force $F_{z,i}$, tyre/road friction μ_i, and the amount of lateral force $F_{y,i}$ applied to the wheel. By estimating $F_{x,lim,i}$ for each wheel the actuator limits are adjusted for what the tyres can handle. The 'tyre fusion' basically checks if the electrical torque limits for the electric motors, $u_{el,lim,i}$, are above the longitudinal force limits and if so, adjusts the limits to be equal to the tyre force capacity. If the sum of electrical and mechanical torque limits $u_{el,mech,lim,i}$ are more than the tyre force limit, then the mechanical limits are set as the difference between the tyre force limit and the electrical limit. The idea is to always try to give the electric motors the possibility to act within the tyre's limits. In equation form this would look something like

$$\underline{u}_{\mathrm{el},i} = \begin{cases} -\overline{F}_{x,i} R_w, & \text{if } \underline{u}_{\mathrm{el},i} \leq -\overline{F}_{x,i} R_w \\ \underline{u}_{\mathrm{el},i}, & \text{else} \end{cases} \tag{35}$$

$$\overline{u}_{\mathrm{mech},i} = 0 \tag{36}$$

$$\underline{u}_{\mathrm{mech},i} = \begin{cases} 0, & \text{if } \underline{u}_{\mathrm{el},i} \leq -\overline{F}_{x,i} R_w \\ -\overline{F}_{x,i} R_w - \underline{u}_{\mathrm{el},i}, & \text{elseif } (\underline{u}_{\mathrm{el},i} + \underline{u}_{\mathrm{mech},i}) \leq -\overline{F}_{x,i} R_w \\ \underline{u}_{\mathrm{mech},i}, & \text{else} \end{cases} \tag{37}$$

where $\underline{u}_{\mathrm{el},i}$ and $\overline{u}_{\mathrm{mech},i}$ are the tyre limits on electrical and mechanical braking torques. The traction torque limits are derived in similar manner. The steering angles are also limited by how much lateral force is still available when actual longitudinal force and its limits are considered.

2) Control Effectiveness matrix B: Here the idea is to linearize $g(x) \approx B$ where B is called the control effectiveness matrix. As mentioned earlier, the virtual control signals are the global forces. Under the assumption that there are no inertia effects in the driveline nor in the wheels, no weak drive shafts, no losses and no time delays or nonlinearities in developing tyre forces, a constant control effectiveness matrix can be formulated. The assumptions are realistic for the control design phase, i.e. the actuators are assumed to be fast. The matrix for the studied configuration becomes

$$B = \begin{bmatrix} \frac{r_{fg}}{R_w} & \frac{r_{fg}}{R_w} & \frac{r_{fg}}{R_w} & \frac{r_{fg}}{R_w} & \frac{1}{R_w} & \frac{1}{R_w} & \frac{1}{R_w} & \frac{1}{R_w} & 0 & 0 \\ 0 & 0 & 0 & 0 & 0 & 0 & 0 & 0 & 2C_\alpha & 2C_\alpha \\ \frac{r_{fg} b_t}{2R_w} & \frac{-r_{fg} b_t}{2R_w} & \frac{r_{fg} b_t}{2R_w} & \frac{-r_{fg} b_t}{2R_w} & \frac{b_t}{2R_w} & \frac{-b_t}{2R_w} & \frac{b_t}{2R_w} & \frac{-b_t}{2R_w} & 2L_f C_\alpha & -2L_r C_\alpha \end{bmatrix} \tag{38}$$

where r_{fg} is the final gear, R_w is the wheel radius, and b_t is the track width. The control effectiveness matrix B describes how the global forces of the vehicle can be generated by the available motion actuators. Observe how many ways the moment M_z, row 3 in B, can be generated which clearly illustrates the over actuation of the vehicle system.

3) Weight Scheduling of $W_u(v)$: Mechanical braking in conventional cars has a certain brake load distribution on the front and rear axles just to ensure vehicle stability during braking. If a vehicle have additional electric motors that will be used during regenerative braking they should also obey similar brake load distribution settings as the mechanical brakes. For example, if a vehicle have large electric motors mounted only on the rear wheels and they are solely used during braking to maximize the regenerative braking it will result in that all of the brake load is taken up on the rear wheels. This will lead to instability and if conditions rapidly change such as friction or in combination when turning. This would almost be an example of the classic 'use the parking brakes to turn' maneuver. For the configuration studied here, the use of electric motors are penalized in the rear more than for the front during braking as is described by

$$W_{u,brake} = \text{diag}[\ 0.1\ 0.1\ 0.3\ 0.3\ 0.5\ 0.5\ 1\ 1\ 1e3\ 2e3\ ]. \tag{39}$$

The opposite load force distribution of the electric motors is found to be desirable during traction to ensure vehicle stability, accordingly

$$W_{u,trac} = \text{diag}[\ 0.3\ 0.3\ 0.1\ 0.1\ 0.5\ 0.5\ 1\ 1\ 1e3\ 2e3\ ]. \tag{40}$$

To handle this efficiently in the control system, the following weight scheduling by linear interpolation of v_1 is suggested

$$W_{u,1,1} = W_{u,2,2} = 0.1, \text{ if } v_1 \leq 0 \tag{41}$$

$$W_{u,3,3} = W_{u,4,4} = 0.1 + \frac{0.3-0.1}{-1g}\frac{v_1}{mg}, \text{ if } v_1 \leq 0 \tag{42}$$

$$W_{u,1,1} = W_{u,2,2} = 0.1 + \frac{0.3-0.1}{1g}\frac{v_1}{mg}, \text{ if } v_1 \geq 0 \tag{43}$$

$$W_{u,3,3} = W_{u,4,4} = 0.1, \text{ if } v_1 \geq 0 \tag{44}$$

where v_1 is the desired longitudinal force, see also Fig. 3.

IV. SIMULATIONS

The selected test procedures are trying to come close to vehicle motion limits, and therefore lead to the fact that arbitration is needed in between the vehicle motion, energy management, and steering laws. The aim is to show that the arbitration is handled smoothly by the control allocator, see Eqs. 30, 31, and 32.

The vehicle system models are implemented as s-functions in Matlab/Simulink. The used control allocator, weighted least squares wls and sequential least squares sls with constraints solvers were coded by [3]. The code was modified by the authors to allow weight scheduling of Wu as a function of the desired virtual signals v and dynamical change in constraints u_{lim}.

A. Test procedures

The following two test procedures were selected for simulation:

TP-A: The purpose is to drive in a circle with a constant radius of 200 m on ice with friction 0.3. The initial velocity was set to 1 m/s. The vehicle is accelerated with 0.1g until 90 percent of the limiting velocity, $v_{lim} = \sqrt{\mu \cdot g \cdot R} = 24.26$ m/s, is reached. Then the velocity is kept constant for 5 s. The final part is braking with -0.1g until reaching 1 m/s as stop velocity. During the whole procedure the aim is to keep the driving circle radius constant.

TP-B: The purpose is to change the deceleration during straight braking on asphalt with friction 1.0. The initial velocity was set to 27.78 m/s. First part is soft braking with -0.1g until 80 km/h is reached then hard braking applied with -0.8g until 11.11 m/s is reached. The final part of the braking is performed again with -0.1g until standstill.

V. RESULTS

A. TP-A results

In Fig. 5 the reference velocities are compared with actual velocities for the sls solution. When 90 percent of the limiting velocity v_{lim} is reached one can see on the yaw rate that the vehicle becomes unstable and stays that way until the braking phase has started and reduced the velocity to about 12 m/s. The desired input signals u_{des} and actual input signals u for the wheel motors and front and rear steering are shown in Fig. 6. The input signals for the disc brakes are not shown because they are not used at all during this test procedure. It can be seen that both the front and rear steering is saturated when 90 percent of the limiting velocity is reached. The limits for the actuators in the plots does not only account for actuator limits but also the tyre force limits. The desired input signals u_{des} are smoothly followed by the wheel motors except for when the steering limits are reached in that time, about 20 s. Motors 1 and 3 then jump up and try to compensate for the loss of steering capability.

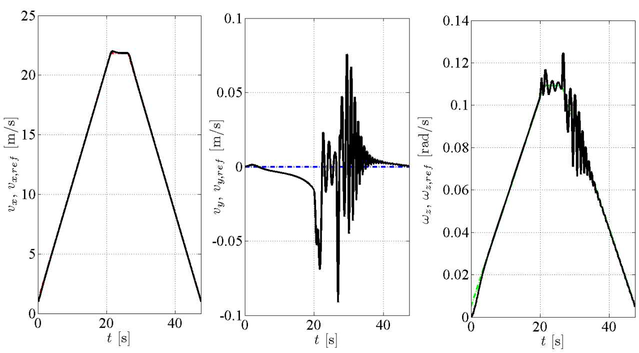

Fig. 5. Reference and actual longitudinal v_x, lateral v_y, and yaw ω_z velocity for sls solution for TP-A.

The constant radius on ice test procedure was used for a sensitivity analysis of the weighting parameter γ found in the wls solver, see Eq. 32 and also for comparing with the sls solver. The comparison was made by studying the least mean squares error, $mse = \frac{1}{n}\sum_{i=1}^{n} e(i)^2$, of the desired path compared with the actual states of the vehicle $e = r - x$, the least mean squares error for the desired motion actuator signals and the actual signals $e = u_{des} - u$. The results are shown in Table I. The wls solver is very robust and quite insensitive when the γ value is varied. When the γ value is varied between $1 \cdot 10^7$ and $1 \cdot 10^{-3}$ only small changes can be observed in results. However when it is lowered to

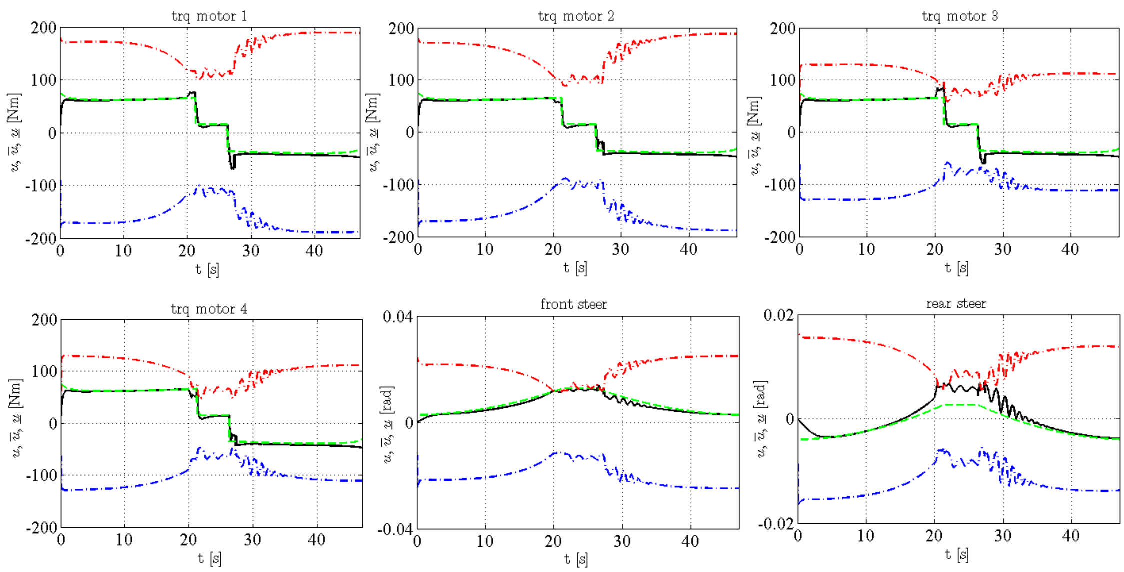

Fig. 6. Input set u and their limits u_{des} during TP-A. The black solid line corresponds to actual u, the dashed green line corresponds to desired u_{des}, and the dotted/dashed red and blue lines are the upper and lower combined limits, respectively.

$\gamma = 1 \cdot 10^{-4}$, both the path and actuator errors jumps. For this test procedure the sls solver outperformed the wls.

TABLE I

SENSITIVITY ANALYSIS OF γ FOR WLS AND COMPARISON WITH SLS FOR TP-A.

solver	γ	mse_{path}	mse_{act}
wls	$1 \cdot 10^{7}$	$7.887 \cdot 10^{-4}$	34.383
wls	$1 \cdot 10^{6}$	$7.882 \cdot 10^{-4}$	34.383
wls	$1 \cdot 10^{5}$	$7.880 \cdot 10^{-4}$	34.383
wls	$1 \cdot 10^{4}$	$7.880 \cdot 10^{-4}$	34.383
wls	$1 \cdot 10^{3}$	$7.881 \cdot 10^{-4}$	34.383
wls	$1 \cdot 10^{2}$	$7.888 \cdot 10^{-4}$	34.383
wls	$1 \cdot 10^{1}$	$7.887 \cdot 10^{-4}$	34.382
wls	$1 \cdot 10^{0}$	$7.871 \cdot 10^{-4}$	34.375
wls	$1 \cdot 10^{-1}$	$7.888 \cdot 10^{-4}$	34.288
wls	$1 \cdot 10^{-2}$	$8.068 \cdot 10^{-4}$	33.214
wls	$1 \cdot 10^{-3}$	$9.447 \cdot 10^{-4}$	26.823
wls	$1 \cdot 10^{-4}$	1.600	189.898
sls	-	$7.868 \cdot 10^{-4}$	21.218

B. TP-B results

The straight braking on asphalt test procedure is simulated both with the wls ($\gamma = 1 \cdot 10^{6}$) and sls solvers. Only small differences can be seen in the results when the least mean squares error is studied for the path and actuator signals. However, this time the wls solver turned out to be slightly better in both path and actuator signal errors.

The reference velocities and actual velocities for TP-B are shown in Fig. 7. One can see the fast response when the braking acceleration is increased from 0.1g to 0.8g. When the braking acceleration is reduced again to 0.1g, at about 7s, the actual longitudinal velocity slightly overshoots.

The desired and actual input signals for wheel motors and disc brakes are shown in Fig. 8. The steering input signals are neglected because no steering is needed in this test procedure. The overshoot in velocity is due to the fact that the rate limits of the mechanical disc brakes takes some time to release the brake pressure. This is however attempted to be compensated for by the wheel motors giving a positive torque at about 8s.

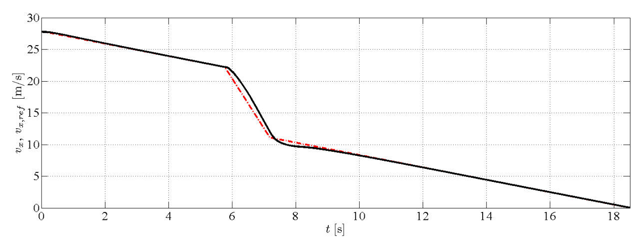

Fig. 7. Reference and actual longitudinal v_x velocity for wls solution for TP-B.

The desired input signals u_{des} from energy management for the wheel motors are smoothly followed whenever this is allowed by the combined limits and providing that the vehicle is following the desired path, see also Fig. 8. However, the desired input signals from energy management for the disc brakes were poorly followed and there are two major reasons for this. Firstly, the combined limits of the actuators and tyre forces did not allow for any other solution. Secondly the weight scheduling $Wu(v)$ requires more load force on front axle than on the rear axle during braking to achieve vehicle stability.

VI. CONCLUSIONS

This paper shows by modelling and simulation that the coordination of control laws for energy management, steering, and vehicle motion can be achieved smoothly by using

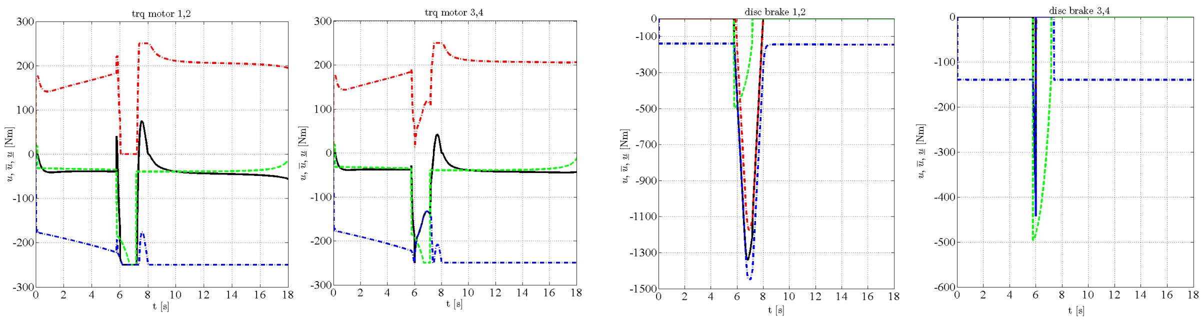

Fig. 8. Input set u for the wheel motors (left plots) and mechanical brakes (right plots) and their limits u_{des} during TP-B. The black solid line corresponds to actual u, the dashed green line corresponds to desired u_{des}, and the dotted/dashed red and blue lines are the upper and lower combined limits, respectively.

control allocation within the control system. Simulations show that whenever possible the desired input u_{des} from energy management and steering is followed. When needed, the actual input u is smoothly diverted to ensure vehicle stability and obey the combined limits of the actuators and tyre forces. The smooth coordination is essential for hybrid electric vehicles where energy management has a long time planning horizon and the vehicle motion controller has a shorter planning horizon.

VII. ACKNOWLEDGMENTS

Bengt Schmidtbauer, Professor Emeritus, is greatly acknowledged for his interest and guidance. The authors would also like to thank the Swedish national research programme Gröna Bilen.

REFERENCES

[1] A. Kimura, T. Abe, and S. Sasaki, "Drive force control of a parallel-series hybrid system," *Society of Automotive Engineers of Japan JSAE Rev. 20,pp. 337–341*, 1999.

[2] A. Emadi, S. Williamson, and A. Khaligh, "Power electronics intensive solutions for advanced electric, hybrid electric, and fuel cell vehicular power systems," *Power Electronics, IEEE Transactions on Vol. 21, Iss. 3, pp. 567–577*, 2006.

[3] O. Härkegård, "Backstepping and control allocation with applications to flight control," Ph.D. dissertation, Department of Electrical Engineering, Linköping University, SE–581 83 Linköping, Sweden, May 2003.

[4] T. Johansen, T. Fossen, and S. P. Berge, "Constrained nonlinear control allocation with singularity avoidance using sequential quadratic programming," *IEEE Transactions on Control Systems Technology, vol. 12, no. 1*, 2004.

[5] T. Johansen, T. Fuglseth, P. Tøndel, and T. I. Fossen, "Optimal constrained control allocation in marine surface vessels with rudders," in *IFAC Conf. Manoeuvring and Control of Marine Craft*, Girona, 2003.

[6] P. Tøndel and T. A. Johansen, "Control allocation for yaw stabilization in automotive vehicles using multiparametric nonlinear programming," in *Proc. of American Control Conf.*, Portland, OR, June 2005.

[7] J. Plumlee, D. Bevly, and A. Hodel, "Control of a ground vehicle using quadratic programming based control allocation techniques," in *Proc. of American Control Conf.*, Boston, MA, July 2004.

[8] J. Plumlee, *Mult-Input Ground Vehicle Control Using Quadratic Programming Based Control Allocation*. Master thesis report, Auburn University, Alabama, 2004.

[9] J. Andreasson, L. Laine, and J. Fredriksson, "Evaluation of a generic vehicle motion control architecture," in *The Fédération Internationale des Sociétés d'Ingénieurs des Techniques de l'Automobile (FISITA)*, Barcelona, Spain, May 2004.

[10] J. Fredriksson, J. Andreasson, and L. Laine, "Wheel force distribution for improved handling in a hybrid electric vehicle using nonlinear control," in *Proceedings of 43rd IEEE Conference on Decision and Control*, Bahamas, December 2004.

[11] SAE, "Surface vehicle recommended practice, vehicle dynamics terminology," *SAE 1976-07, J670e*, 1976.

[12] H. B. Pacejka, *Tyre And Vehicle Dynamics 2^{nd} edition*. Butterworth-Heinemann, 2002.

[13] M. Schenck, J.-S. Lai, and K. Stanton, "Fuel cell and power conditioning system interaction," in *Applied Power Electronics Conference and Exposition, APEC 2005, 20th Annual Conference of IEEE*, March 2005.

[14] J. Marshall and M. Kazerani, "Design of an efficient fuel cell vehicle drivetrain, featuring a novel boost converter," in *Industrial Electronics Society, IECON 2005, 32nd Annual Conference of IEEE*, November 2005.

[15] R. Spotnitz, "Advanced ev and hev batteries," in *Vehicle Power and Propulsion, 2005 IEEE Conference*, Sept. 2005.

[16] H. Khalil, *Nonlinear Systems, 3^{rd} edition*. Prentice Hall Inc., 2002.

[17] K. Åström and T. Hägglund, *PID Controllers: Theory, Design, and Tuning*. Instrument Society of America, 1995.

[18] J. Schiffer, O. Bohlen, R. D. Doncker, D. U. Sauer, and K. Ahn, "Optimized energy management for fuelcell-supercap hybrid electric vehicles," in *Vehicle Power and Propulsion, 2005 IEEE Conference*, Sept. 2005.